JACS
JOURNAL OF THE AMERICAN CHEMICAL SOCIETY
Article
pubs.acs.org/JACS

Transition from Molecular Vibrations to Phonons in Atomically Precise Cadmium Selenide Quantum Dots

Alexander N. Beecher,[‡] Rachel A. Dziatko,[†] Michael L. Steigerwald,[‡] Jonathan S. Owen,[‡] and Andrew C. Crowther*[,†]

[†]Department of Chemistry, Barnard College, New York, New York 10027, United States
[‡]Department of Chemistry, Columbia University, New York, New York 10027, United States

Supporting Information

ABSTRACT: We use micro-Raman spectroscopy to measure the vibrational structure of the atomically precise cadmium selenide quantum dots $Cd_{35}Se_{20}X_{30}L_{30}$, $Cd_{56}Se_{35}X_{42}L_{42}$, and $Cd_{84}Se_{56}X_{56}L_{56}$. These quantum dots have benzoate (X) and *n*-butylamine (L) ligands and tetrahedral (T_d) shape with edges that range from 1.7 to 2.6 nm in length. Investigating this previously unexplored size regime allows us to identify the transition from molecular vibrations to bulk phonons in cadmium selenide quantum dots for the first time. Room-temperature Raman spectra have broad CdSe peaks at 175 and 200 cm^{-1}. Density functional theory calculations assign these peaks to molecular surface and interior vibrational modes, respectively, and show that the interior, surface, and ligand atom motion is strongly coupled. The interior peak intensity increases relative to the surface peak as the cluster size increases due to the relative increase in the polarizability of interior modes with quantum dot size. The Raman spectra do not change with temperature for molecular $Cd_{35}Se_{20}X_{30}L_{30}$, while the interior peak narrows and shifts to higher energy as temperature decreases for $Cd_{84}Se_{56}X_{56}L_{56}$, a spectral evolution typical of a phonon. This result shows that the single bulk unit cell contained within $Cd_{84}Se_{56}X_{56}L_{56}$ is sufficient to apply a phonon confinement model, and that $Cd_{56}Se_{35}X_{42}L_{42}$, with its 2.1 nm edge length, marks the boundary between molecular vibrations and phonons.

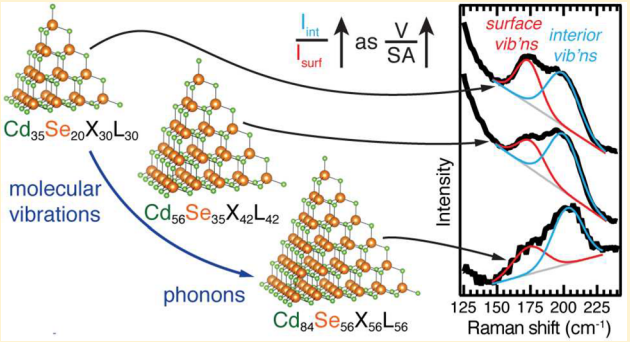

1. INTRODUCTION

Quantum dots (QDs) occupy a crucial size regime for understanding how the properties of semiconductors change from the bulk to the molecular limit. For example, in QDs, excitons are confined, and the electronic structure begins to possess the discretized states characteristic of molecules.[1,2] While the size dependence of the electronic structure is well-understood,[2,3] investigations of QD vibrational structure have focused on either the molecular or bulk limits, rather than the transition region between them. These studies use two general approaches: a quantum chemical, molecular normal mode model that treats a small nanocrystal as an assembly of atoms built from the bottom up,[4] and a phonon confinement model that treats nanocrystals as small crystalline fragments cut out from the bulk material.[5−7] Both of these models are valid, with the molecular approach performing better for clusters that are composed primarily of surface atoms,[4] and the phonon confinement model accurately describing the vibrational structure of larger crystallites that have an interior lattice structure.[8] However, the size-dependent transition from molecular vibrations to phonons is not well-understood due to a lack of high quality samples in the appropriate size regime. We overcome this challenge by performing low-frequency Raman experiments on a series of recently reported, atomically precise cadmium selenide QDs that have well-defined structures and small sizes. These QDs enable us to determine how molecular vibrations evolve into the phonons of an extended solid and to understand the physical basis for the transition between these two limits.

We investigate a structurally characterized class of tetrahedral cadmium selenide QDs (Figure 1).[9] These samples retain the characteristic properties of more conventional spherical QDs, such as size-dependent absorption and photoluminescence, metal-rich stoichiometries, and carboxylate and amine passivation, but they assume structures that are atomically precise in size and shape with edge lengths between 1.7 and 2.6 nm. We have previously determined their formulas, $Cd_{35}Se_{20}X_{30}L_{30}$, $Cd_{56}Se_{35}X_{42}L_{42}$, and $Cd_{84}Se_{56}X_{56}L_{56}$, where X is benzoate and L is *n*-butylamine.[9] For simplicity, we will call the samples **CdSe**$_{(350\ nm)}$, **CdSe**$_{(380\ nm)}$, and **CdSe**$_{(408\ nm)}$ after the wavelengths of their lowest energy electronic transitions. We will also call our atomically precise QD samples "clusters", to distinguish them from larger, spherical nanocrystals.

Previous Raman studies have characterized many aspects of CdSe QD vibrational structure, including the interfacial

Received: October 12, 2016
Published: December 16, 2016

DOI: 10.1021/jacs.6b10705
J. Am. Chem. Soc. 2016, 138, 16754−16763

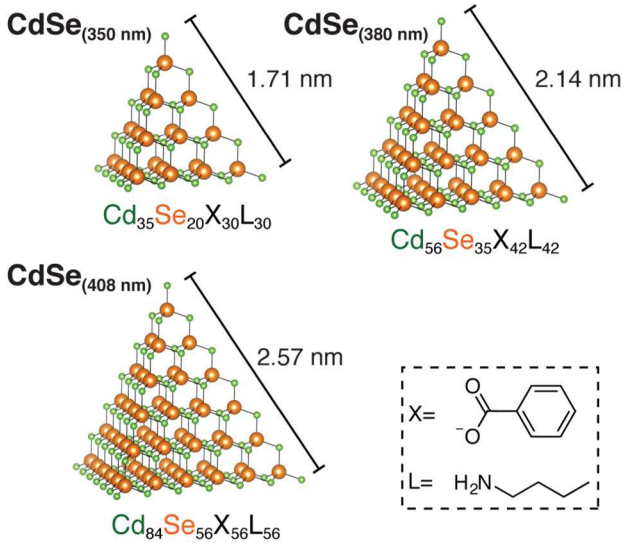

Figure 1. Three atomically precise, tetrahedral cadmium selenide QDs possessing known formulas and discrete dimensions with edge lengths ranging from 1.7 to 2.6 nm in size. The X and L type ligands are benzoate and *n*-butylamine, respectively.

structure of core−shell nanocrystals[10−13] and the coupling between vibrational and electronic states.[6,8,14−16] These experiments typically study QDs with $d \geq 3$ nm and rely upon a phonon confinement model. This model is based on the vibrational structure of bulk wurtzite CdSe, which has C_{6v} symmetry and nine optical phonon branches,[17] including the Raman active longitudinal optical (LO) and transverse optical (TO) branches.[18−20] Nonresonant Raman scattering experiments on bulk CdSe detect peaks corresponding to the LO mode at 211 cm^{-1} and the TO mode at 169 cm^{-1},[20,21] but because first-order Raman scattering is only allowed near the zero momentum Γ point, measurements do not detect the rest of the phonon branch.[5] According to the phonon confinement model, the momentum selection rules relax at small dimensions, and more of the phonon dispersion curve becomes Raman allowed. This model predicts a broadening and shift to lower energy of the Raman peak for phonon bands with negative dispersion, although strain due to lattice contraction can partially offset the frequency shift.[10,22−24] Indeed, in the spectra of CdSe QDs, the LO mode broadens and shifts to lower energy relative to the bulk while the TO mode is typically absent.[8,25,26] An additional difference between nanocrystal and bulk Raman spectra involves a lower energy shoulder on the LO mode at approximately 195 cm^{-1} for CdSe QDs. This peak is commonly assigned to a surface optical (SO) mode, which corresponds to lower energy vibrations of surface atoms.[23,27−29]

Phonon confinement models have limited utility at very small dimensions. For example, *ab initio* calculations performed on CdS QDs embedded in a glassy matrix show that the vibrational modes have mixed, rather than pure, LO, TO, and SO character.[30] Similarly, calculations on zincblende CdS nanocrystals ($d = 3.6$ nm) showed that the Cd−S stretch Raman peak at ∼350 cm^{-1}, commonly labeled the LO mode, possesses both TO and LO character.[31] Finally, force field calculations on CdSe QDs ($d = 3.2$ nm) show that the SO mode at ∼195 cm^{-1} is not localized on the surface, but is composed of vibrations that extend throughout the nanocrystal.[29]

In contrast to the top-down phonon confinement approach, molecular normal mode analysis has been used to interpret the Raman spectra of clusters.[4,32,33] Clusters and nanocrystals composed of tens to hundreds of atoms have many Raman allowed normal modes of slightly different energies that combine to produce the overall vibrational spectrum. For example, Løver et al. measured the infrared and Raman spectra of thiophenolate-capped cadmium sulfide clusters that range in size from $d = 1$ to 4 nm and observed several broad signals in the CdS stretching region.[4] They assign the lower energy features to cadmium-thiophenolate-derived vibrations where the thiophenolate ligand moves as a rigid body, while the higher energy feature is attributed to a distribution of stretching motions of Cd−S bonds within the cluster's interior.[4]

Inspired by this work, we adopt a molecular perspective in this study because, while our clusters share many similarities with larger, spherical quantum dots, their dimensions are substantially reduced. In our size range ($d = 1.7$ to 2.6 nm), molecular normal modes are successful at treating the vibrations of large clusters, and the observed Raman features are not readily assignable to specific phonon modes. Our samples are well-suited to such a molecular analysis because they have known formulas and atomically precise structures.[34] Thus, we expect our Raman peaks to be bands of many molecular vibrations, rather than a few momentum allowed phonons.

In this paper, we use micro-Raman spectroscopy to investigate the vibrational structure of a series of three atomically precise CdSe QDs. We also measure the spectra of wurtzite and zincblende CdSe nanocrystals (**CdSe**$_{(Wz\ NCs)}$ and **CdSe**$_{(Zb\ NCs)}$), and bulk wurtzite-phase CdSe (**CdSe**$_{(Bulk)}$) for comparison. We conduct experiments using two laser wavelengths to study resonance effects, and we perform variable-temperature measurements to investigate the evolution from molecular vibrations to bulk phonons. Finally, we support our experimental results with density functional theory (DFT) calculations of the vibrational structure of the atomically precise QDs. Our results show that a molecular analysis effectively describes the vibrational structure of our samples and allows us to confidently assign the observed CdSe stretching modes to surface and interior vibrations. Surprisingly, temperature-dependent measurements show that the single bulk zincblende unit cell present in the largest atomically precise QD that we study, **CdSe**$_{(408\ nm)}$, is sufficient to successfully apply the phonon confinement model typically used on larger spherical nanocrystals. In contrast, the smaller **CdSe**$_{(350\ nm)}$ is composed of molecular normal modes, showing that **CdSe**$_{(380\ nm)}$, with its 2.1 nm edge length, is the size at which the QD vibration structure begins to resemble bulk phonons.

2. EXPERIMENTAL SECTION

2.1. General Considerations. Most reagents were acquired and treated as reported by Beecher et al.[9] Additionally, cadmium selenide (10 μm, 99.99%), octadecene (90%), and oleic acid (99%) were purchased from Sigma-Aldrich and used as received. Anhydrous methyl acetate (99.5%) was purchased from Sigma-Aldrich, shaken with activated alumina, filtered, and stored over 4 Å molecular sieves for at least 24 h prior to use. Cadmium oxide (99.99+%) and tri-*n*-octylphosphine (>99.7%) were purchased from Strem and used as received. Tri-*n*-octylphosphine oxide was purchased from Aldrich and recrystallized according to previously reported procedures.[35] Cadmium benzoate ($Cd(C_7H_5O_2)_2{\cdot}(CH_3CN)_{0.2-0.3}$), bis(trimethylsilyl)selenide ($Se(Si(CH_3)_3)_2$), and cadmium tetradeconoate were all prepared following literature procedures.[9,36] The synthesis of *n*-octadecylphosphonic acid used in the preparation of **CdSe**$_{(Wz\ NCs)}$ is reported in the Supporting Information.

DOI: 10.1021/jacs.6b10705
J. Am. Chem. Soc. 2016, 138, 16754−16763

Unless otherwise indicated, all manipulations were performed under air-free conditions using standard Schlenk techniques or a nitrogen atmosphere glovebox. These techniques ensure that the samples do not oxidize, which we confirm using elemental and XRD characterization methods.[9] NMR spectra were recorded on Bruker Advance III 400 and 500 MHz instruments and internally referenced to the resonances of protio-impurities in the deuterated solvent. ^{1}H NMR spectra were acquired with sufficient delay to allow complete relaxation between pulses (15 s). UV−visible absorption data were obtained using a PerkinElmer Lambda 650 spectrophotometer equipped with deuterium and tungsten halogen lamps. Photoluminescence spectra were recorded using a FluoroMax-4 from Horiba Scientific. Cluster structural models were generated in Vesta.[37]

2.2. Synthesis. *Synthesis and isolation of $CdSe_{(350\ nm)}$, $CdSe_{(380\ nm)}$, and $CdSe_{(408\ nm)}$.* The set of cluster samples was synthesized using a previously reported procedure without modification.[9]

Synthesis of wurtzite CdSe nanocrystals. *n*-Octadecylphosphonate-terminated wurtzite nanocrystals were prepared by following a previously reported procedure.[38] To achieve the desired size (3.0 nm in diameter using the sizing formula reported by Beecher et al.),[9] the reaction was halted after 2.5 min at 370 °C. The crystals were purified in an air-free manner following a previously reported procedure using methyl acetate in place of acetone, toluene in place of chloroform, and pentane in place of hexane.[35] The samples were characterized by UV−visible and NMR spectroscopies to determine whether the sample was free of impurities.

Synthesis of zincblende CdSe nanocrystals. Carboxylate-terminated zincblende CdSe nanocrystals were synthesized, purified, and characterized via previously reported methods.[36] The nanocrystals used for the reported measurements are 3.25 nm in diameter.

2.3. Raman Spectroscopy. Working in a nitrogen-filled glovebox to avoid air exposure, samples were prepared by dissolving the material of interest in toluene (approximately 10 mg in 0.5 mL of toluene) and drop-casting onto a fragment of silicon wafer (~5 × 5 mm) to form a thin film that is visible by eye. Samples were loaded into quartz cuvettes and sealed before bringing the samples to the Raman spectrometer.

A micro-Raman spectrometer measured CdSe samples with 532 and 633 nm lasers. For our measurements, 2 mW of 532 nm or 3.6 mW of 633 nm light enters a Nikon Eclipse Ti/U inverted microscope, and a 30%R/70%T broadband beamsplitter directs the light into a 40×/0.6 N.A. objective, which focuses the light to a ~1 μm diameter spot on the sample. Backscattered light collected by the same objective passes through a 75 μm confocal pinhole, through a long pass filter, and into a 300 mm Acton SP2300 spectrometer with a 1200 g/mm grating before reaching a Pixis 400 CCD imaging detector. The resolution for measurements with λ_{exc} = 532 nm is 5.2 ± 0.5 cm^{-1}, determined from the 546 nm peak of a Hg calibration lamp. The resolution for measurement with λ_{exc} = 633 nm is 3.8 ± 0.5 cm^{-1}, determined from the 638.3 nm peak of a Ne calibration lamp.

The Raman spectra of $\mathbf{CdSe_{(350\ nm)}}$, $\mathbf{CdSe_{(380\ nm)}}$, $\mathbf{CdSe_{(408\ nm)}}$, $\mathbf{CdSe_{(Wz\ NCs)}}$, $\mathbf{CdSe_{(Zb\ NCs)}}$, and $Cd(O_2CPh)_2(n\text{-}BuNH_2)_2$ were measured with λ_{exc} = 532 nm and λ_{exc} = 633 nm. $Cd(O_2CPh)_2(n\text{-}BuNH_2)_2$ was used to approximate the benzoate and *n*-butylamine ligands in the cluster samples and was produced by drop-casting a toluene solution containing $Cd(O_2CPh)_2$ and 2 equiv of *n*-butylamine onto a silicon substrate. For $\mathbf{CdSe_{(Bulk)}}$, we only conduct measurements with λ_{exc} = 532 nm due to sample fluorescence in the detection region of measurements with λ_{exc} = 633 nm. Even minor sample fluorescence can saturate the detector, so we routinely performed many shorter scans in order to increase total acquisition time. For λ_{exc} = 532 nm, typical *total* acquisition times were 4−32 min for the CdSe clusters and bulk samples and 1−5 min for the nanocrystal and $Cd(O_2CPh)_2(n\text{-}BuNH_2)_2$ samples. Measurements performed with λ_{exc} = 633 nm used exposure times of 10−60 min for the CdSe clusters and 5−13 min for the nanocrystal and $Cd(O_2CPh)_2(n\text{-}BuNH_2)_2$ samples.

Variable-temperature measurements were acquired using the 532 nm laser to maximize the signal-to-noise ratio. Samples were loaded into an Oxford Instruments Microstat HiRes2 cryostat in the glovebox, and a Varian Turbo-V70 turbo pump backed by an Agilent TriScroll dry vacuum roughing pump evacuated the cryostat. Temperature was controlled with an Oxford Instruments Mercury iTC controller and a cold nitrogen stream. We measured Raman spectra of $\mathbf{CdSe_{(350\ nm)}}$, $\mathbf{CdSe_{(380\ nm)}}$, $\mathbf{CdSe_{(408\ nm)}}$, and $Cd(O_2CPh)_2(n\text{-}BuNH_2)$ at 294, 250, 200, 150, 100, and 78 K. The cooling rate was approximately 5 K/min. Typical total acquisition times for variable-temperature measurements were 20 min.

2.4. Calculations. We performed density functional theory calculations using Jaguar.[39] Geometries were optimized, orbitals were calculated, and energies were determined at the B3LYP/LACVP** level.[40−43] We generated cluster models based on the reported structures and formulas by substituting chlorides for benzoates and ammonias for *n*-butylamines, which are approximations of the original ligands, but are not as computationally expensive. In addition, the excess Cd^{2+} relative to Se^{2-} in each cluster requires that we replace the anionic benzoate ligands with chloride to maintain charge balance, keeping the overall cluster neutral. Calculations were performed on three molecules: $Cd_{20}Se_{10}Cl_{20}(NH_3)_{20}$, $Cd_{35}Se_{20}Cl_{30}(NH_3)_{30}$ for $\mathbf{CdSe_{(350\ nm)}}$, and $Cd_{56}Se_{35}Cl_{42}(NH_3)_{42}$ for $\mathbf{CdSe_{(380\ nm)}}$. $Cd_{20}Se_{10}Cl_{20}(NH_3)_{20}$ is one layer smaller than $\mathbf{CdSe_{(350\ nm)}}$, consistent with the size trend in Figure 1. We produced three different regioisomers of the $Cd_{20}Se_{10}Cl_{20}(NH_3)_{20}$ model by rearranging the ligands such that in the two more symmetric versions all faces present an even mixture of chloride and ammonia ligation (dipole moment = ~5.5 D) while the more asymmetric version possesses faces enriched in either ammonia or chloride ligands (dipole moment = ~19 D) (Figure S6). Calculations for larger clusters used symmetric, evenly distributed ligand placements. These geometries were then optimized before performing further calculations. We processed the extracted vibrational data by assigning each atom to one of three categories, interior, surface, or ligand, and then determining the magnitude of every atom's displacement for each vibrational mode. We define a surface atom as a cadmium that forms bonds with chloride or ammonia ligands, interior atoms as any other cadmium or selenium, and ligand atoms as all chlorines, nitrogens, and hydrogens.

3. RESULTS AND DISCUSSION

By studying a set of well-defined samples at the interface of discrete small molecules and nanocrystals, we seek to a) understand how molecular vibrations become phonons as nanocrystals increase in size and b) determine the physical origin of the boundary between the size regime where vibrational structure is best described using a molecular vibrational mode analysis and where a phonon confinement model is more appropriate.

To answer these questions, we perform Raman measurements with λ_{exc} = 532 and 633 nm on three atomically precise tetrahedral CdSe clusters, spherical zincblende and wurtzite CdSe nanocrystals, and bulk wurtzite CdSe. Figure S1 shows that the absorption and photoluminescence spectra of our clusters have the same size dependence as larger, spherical nanocrystals, despite their tetrahedral shape,[9] and that all cluster Raman measurements are nonresonant. For $\mathbf{CdSe_{(Wz\ NCs)}}$ (d = 3.0 nm) and $\mathbf{CdSe_{(Zb\ NCs)}}$ (d = 3.3 nm), which were prepared using known methods and are passivated by *n*-octadecylphosphonate and *n*-octylamine ligands, respectively,[35,36,38] measurements with λ_{exc} = 633 nm are nonresonant while measurements with λ_{exc} = 532 nm are resonant and excite the samples at slightly higher energies than their lowest energy electronic transitions (Figure S2).

3.1. Room-Temperature Measurements. Figure 2 displays the room-temperature Raman spectra of $\mathbf{CdSe_{(350\ nm)}}$, $\mathbf{CdSe_{(380\ nm)}}$, and $\mathbf{CdSe_{(408\ nm)}}$ with λ_{exc} = 532 and 633 nm. Three important sets of peaks appear in each spectrum: cadmium selenide stretch modes near 200 cm^{-1}, benzoate and *n*-butylamine ligand modes throughout the entire detection

DOI: 10.1021/jacs.6b10705
J. Am. Chem. Soc. 2016, 138, 16754−16763

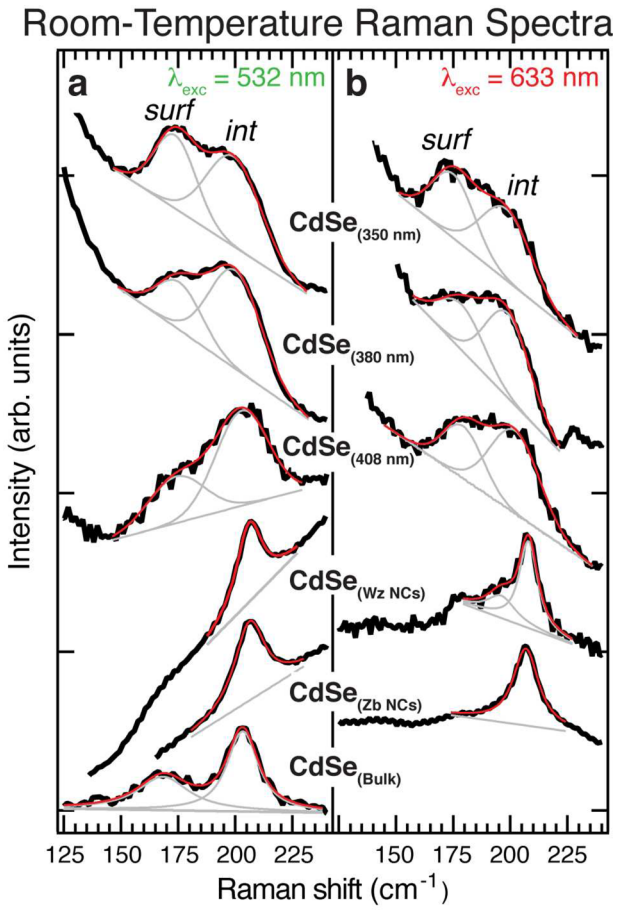

Figure 2. Representative (a) λ_{exc} = 532 nm and (b) λ_{exc} = 633 nm Raman spectra of the clusters, two nanocrystal standards, and bulk wurtzite CdSe. The black, gray, and red curves are the data, individual peak fits, and total fit, respectively. We fit the nanocrystals and bulk spectra to Lorentzian functions and the clusters to Gaussians. The background (gray line) is linear for all spectra.

region (Figure S3), and silicon substrate modes at 300, 520, and 960 cm^{-1} (Figure S3). The CdSe feature contains two broad, overlapping peaks at ~175 cm^{-1} and ~200 cm^{-1}, with the 200 cm^{-1} peak intensity growing relative to the ~175 cm^{-1} peak as the cluster size increases for both laser wavelengths (Figure 2). We observe some fluorescence, mostly for larger clusters with the 532 nm laser (Figure S3). Although the Raman measurements are off-resonance, optical excitation becomes more probable with increasing cluster size as the lowest energy electronic transition approaches the laser wavelength.[44] To account for sample fluorescence and a low-energy sloping feature associated with the ligands, we use a linear background. For details on this background choice, see the Supporting Information.

Previous Raman studies of CdSe and CdS nanocrystals fit the Cd−Se and Cd−S stretch peaks to Lorentzian line shapes,[8,11,12,45] an appropriate approach for larger, more homogeneous systems where the individual vibrational modes have begun to assume a more collective, phonon character.[5] However, fits of the CdSe peaks in our cluster spectra to Lorentzian line shapes were poor. Instead, we fit the CdSe peaks at ~175 cm^{-1} and ~200 cm^{-1} to Gaussians, which are the proper line shapes for inhomogeneously broadened features composed of a wide variety of molecular normal modes. For each cluster size, we measure multiple samples over multiple days and fit each individual spectrum independently. Fit results are in Table S1. This approach generated robust results for the peak positions and widths, with good agreement between measurements performed with 532 and 633 nm excitation. However, for the largest clusters, there was significant covariance between the peak widths and heights, resulting in unreliable peak areas. As a result, we also fit all data (λ_{exc} = 532 and 633 nm) for a given cluster size simultaneously, producing a single set of fitting parameters for each cluster (Table S2). The resulting peak locations and widths matched the individual fits without the corresponding uncertainty in peak area.

For comparison, we also measure the Raman spectrum of $\mathbf{CdSe}_{(Bulk)}$, $\mathbf{CdSe}_{(Wz\ NCs)}$, $\mathbf{CdSe}_{(Zb\ NCs)}$, and the molecular species $(Cd(O_2CPh)_2(n\text{-}BuNH_2)_2)$, which we refer to as "ligand-only". The ligand-only Raman spectrum has a broad sloping feature at 100 cm^{-1} with a very weak peak at 200 cm^{-1} (Figure S4). The low-energy feature likely arises from a broad, inhomogeneous distribution of low-frequency vibrational modes while the weak peak at 200 cm^{-1} is due to Cd−(O_2CPh) motions.[4,46−49] Other ligand features at higher energies in the cluster spectra are sharp, corresponding to C−C stretches, CCH and CCC in-plane deformations, and C−H and C═O out-of-plane deformations, and they closely match the ligand-only control spectrum (Figure S3).[46,48,49] While we must account for the broad background from the ligands in our fits, the peak at 200 cm^{-1} is weak and does not significantly affect our analysis of the CdSe vibrations.

Finally, Figure 2 displays the Raman spectra and fits of $\mathbf{CdSe}_{(Bulk)}$, $\mathbf{CdSe}_{(Wz\ NCs)}$, and $\mathbf{CdSe}_{(Zb\ NCs)}$ samples. As expected for larger samples with a more homogeneous bulk vibrational structure, the CdSe modes of these larger samples are best fit to Lorentzians. In the case of the spectra obtained with λ_{exc} = 532 nm, we find that a single Lorentzian fits each peak very well, with additional Lorentzians only marginally improving the fit. Spectra of $\mathbf{CdSe}_{(Wz\ NCs)}$ obtained with λ_{exc} = 633 nm are better fit using two Lorentzian functions. Similar to previous reports, the $\mathbf{CdSe}_{(Bulk)}$ spectrum has a TO feature at 170 ± 1.5 cm^{-1} and an LO feature at 204 ± 1.0 cm^{-1}.[20,21] This LO value is lower than the typical literature value of 211 cm^{-1}, likely due to local heating from our laser, which is not an issue for our nonresonant cluster Raman spectra.[25] Similarly, all $\mathbf{CdSe}_{(Wz\ NCs)}$ and $\mathbf{CdSe}_{(Zb\ NCs)}$ spectra show an LO mode at ~206 cm^{-1}, and the $\mathbf{CdSe}_{(Wz\ NCs)}$ Raman spectrum with λ_{exc} = 633 nm has a second peak at 195.2 ± 0.9 cm^{-1}, in good agreement with the typical LO and SO literature assignments.[11,14,25] We do not observe the SO peak in the other nanocrystal spectra because the fluorescence obscures the weak shoulder on the LO peak.

Figure 3 shows that both peaks increase in energy with QD size, and exhibit no dependence on laser wavelength, as expected for nonresonant Raman measurements. The higher energy peak frequency increases linearly with size across all clusters and nanocrystals, converging to the typical LO value of 206 cm^{-1} for zincblende nanocrystals. Interestingly, the zincblende clusters and wurtzite and zincblende spherical QDs all follow the same trend, suggesting that these vibrational modes do not depend on the surface. The lower energy peak frequency increases linearly with size for the cluster samples, but jumps from ~180 cm^{-1} to 195 cm^{-1} upon transitioning from the largest cluster, $\mathbf{CdSe}_{(408\ nm)}$, to the smallest QD, $\mathbf{CdSe}_{(Wz\ NCs)}$. In contrast to peak frequency, there is too much uncertainty in our measurements of peak width to confidently establish a trend (Figure S5).

DOI: 10.1021/jacs.6b10705
J. Am. Chem. Soc. 2016, 138, 16754−16763

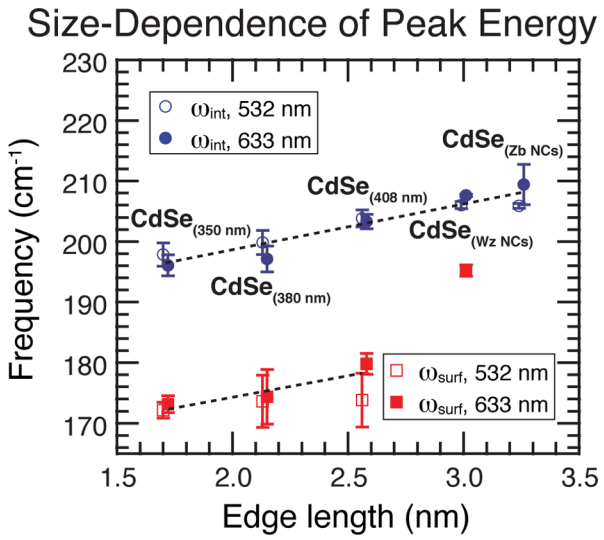

Figure 3. ω_{int} (blue circles) and ω_{surf} (red squares) as a function of size for both λ_{exc} = 532 nm (empty) and λ_{exc} = 633 nm (filled). Markers for each excitation wavelength are slightly offset horizontally for clarity. For the spherical nanocrystals, the "edge length" is the diameter. The dashed lines are uncertainty weighted fits. Linear fits are $\omega_{int} = 7.6x + 183.5$ and $\omega_{surf} = 7.1x + 160.1$.

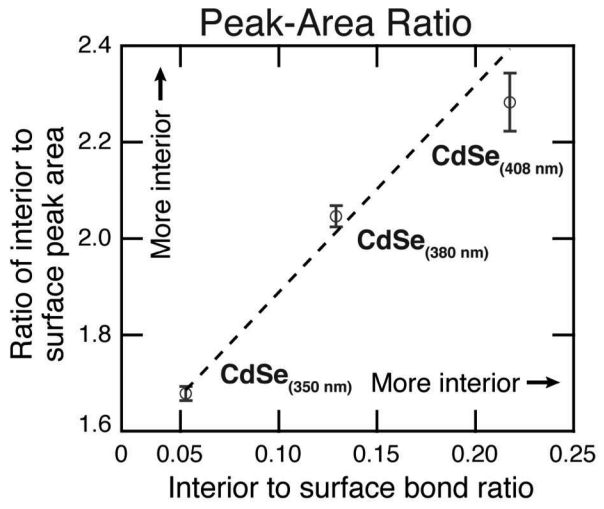

Figure 4. Peak area ratio of the higher energy interior feature to the lower energy surface feature as a function of the ratio of interior to surface bonds. Smaller clusters exhibit a more pronounced surface peak, and larger clusters exhibit a more pronounced interior peak. A surface bond is any bond between an interior Se and a surface Cd, and an interior bond is any bond between two interior Cd and Se atoms. The linear fit equation is $y = 4.3x + 1.46$.

Past studies of large, spherical nanocrystals typically explain the size-dependent shift in the LO mode using a model that includes contributions from phonon confinement and compressive strain.[8,24] Phonon confinement predicts decreased frequency and increased width with decreasing size.[1,5,25] Surface tension induced compressive strain, which is also called lattice contraction, partially counteracts this frequency shift.[8,24] However, a molecular normal mode approach predicts the same size dependence of peak energy and width as the combined phonon confinement and strain model. As particles shrink, more atoms are less rigidly bound in the crystal lattice and vibrations will have lower frequencies. For the same reason, width should simultaneously increase due to greater heterogeneity in the types of vibrations underlying a given feature. Because vibrational modes of the smaller clusters at best weakly resemble the LO and SO modes of a bulk crystal, we use density functional theory calculations to determine the molecular normal modes of the clusters and more definitively assign the Raman peaks.

3.2. Peak Assignments. Proper assignment of the two broad peaks at ~200 cm^{-1} and ~175 cm^{-1} in the room-temperature cluster spectra requires careful consideration of both the size evolution of the spectra and the specific normal mode motions at these energies. The higher energy peak occurs in all cluster, nanocrystal, and bulk samples, while the lower energy peak is present only in the cluster spectra. A typical approach would assign the higher energy peak of the clusters to a mode analogous to the bulk LO phonon mode, and the lower energy peak would be assigned to the SO phonon mode.[23,29] This assignment is consistent with the observation that the area of the higher energy "interior" peak increases relative to the area of the lower energy "surface" peak as the cluster gets larger and the number of interior bonds increases (Figure 4).

We approach these assignments from a molecular perspective, because cluster and nanocrystal vibrations are unlikely to be directly analogous to the optical phonons of the bulk. Most atoms are on the surface, and previous calculations show that the vibrational structure of nanocrystals is more complicated than a phonon model implies.[29−31] Our clusters are ideal candidates for a molecular treatment with density functional theory because they are both atomically precise and relatively small by nanocrystal standards.[50] To probe the origins of the peaks at ~200 cm^{-1} and ~175 cm^{-1}, we performed calculations on three clusters: $Cd_{20}Se_{10}Cl_{20}(NH_3)_{20}$, which is one layer smaller than $\mathbf{CdSe_{(350\ nm)}}$, and $Cd_{35}Se_{20}Cl_{30}(NH_3)_{30}$ and $Cd_{56}Se_{35}Cl_{42}(NH_3)_{42}$, which have the same core formulas as $\mathbf{CdSe_{(350\ nm)}}$ and $\mathbf{CdSe_{(380\ nm)}}$, respectively.[39] We use chloride and ammonia ligands to simulate the native benzoate and *n*-butylamine ligands because they are less computationally expensive while still maintaining cluster charge neutrality. Including ligands provides a better approximation of the true structure but also results in lower cluster symmetry.[50] A previous report calculated the complete Raman spectrum of a similarly sized CdSe magic-size cluster passivated by a single ligand.[51] However, determining the polarizability of fully passivated clusters is challenging, and our efforts to calculate the Raman spectrum were ultimately unsuccessful.

The results of the density functional theory normal mode analysis are shown in Figure 5. The absolute calculated vibrational mode energies are larger than in our Raman spectra, and the standard vibrational frequency scaling factors for our computational method and basis set do not substantially affect the results.[52] However, the relative energies of different vibrational modes are instructive. The vibrational density of states is qualitatively similar for each cluster size and shows that modes are distributed widely and relatively evenly from 50 to 400 cm^{-1} with the exception of a single spike in vibrational density at 250 cm^{-1}, which corresponds to ligand motions (Figure 5a). There is no obvious increase in the relative number of modes at higher energy with increasing cluster size. However, when we decompose the modes of $Cd_{56}Se_{35}Cl_{42}(NH_3)_{42}$ into the motions of the constituent atoms sorted by type (interior cadmium and selenium, surface cadmium, and ligand), we find more interior atom motion at higher energy while surface atom motion is more constant with vibrational energy (Figure 5b).

DOI: 10.1021/jacs.6b10705
J. Am. Chem. Soc. 2016, 138, 16754−16763

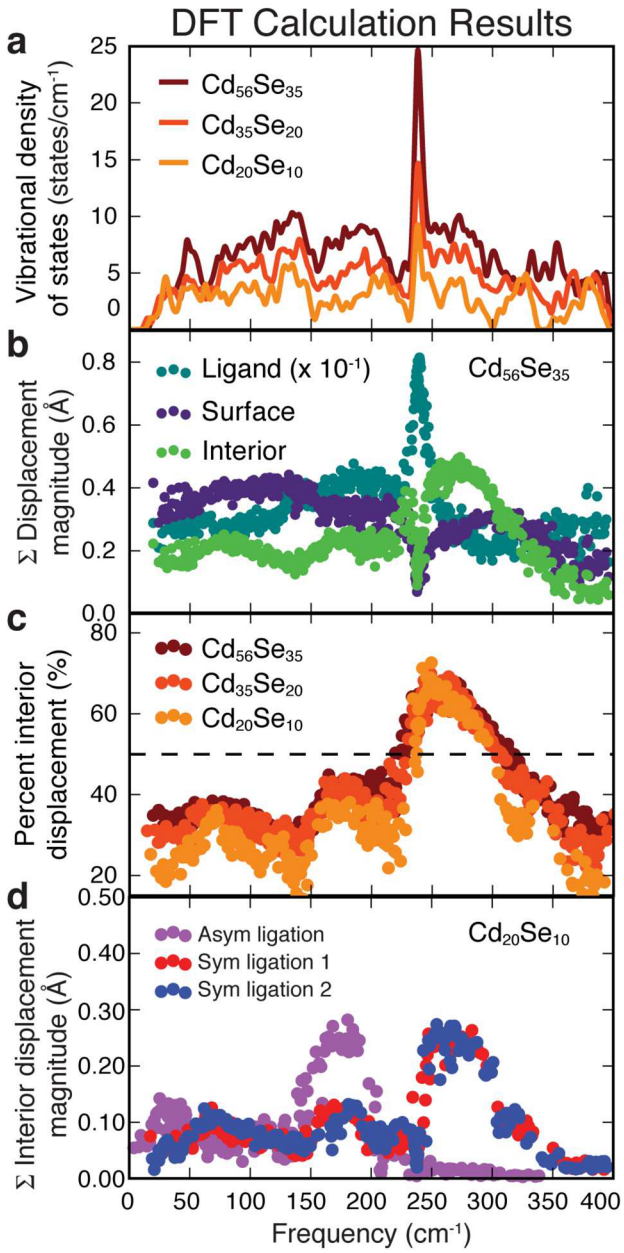

Figure 5. DFT calculation results for $Cd_{20}Se_{10}Cl_{20}(NH_3)_{20}$, $Cd_{35}Se_{20}Cl_{30}(NH_3)_{30}$, and $Cd_{56}Se_{35}Cl_{42}(NH_3)_{42}$. (a) We determine the vibrational density of states (VDOS) for all three clusters by summing Gaussians with $\sigma = 2$ cm^{-1} for each mode and (b) show for one cluster, $Cd_{56}Se_{35}Cl_{42}(NH_3)_{42}$, a decomposition of the displacement magnitude of every atom in each mode by atom type: interior, surface, and ligand. (c) We examine the proportion of Cd and Se atom motions occurring either in the interior or on the surface of the models and (d) find that the arrangement of ligands can strongly affect the motion of all atoms, even those in the interior.

For all modes, the ligands account for roughly 90% of total atomic motion, because the ligand shell contains many light atoms. Ligand motion is also strongly coupled to the cadmium and selenium atoms and vice versa. Visually inspecting the motion of each normal mode reveals complex, highly asymmetric motions that are not easily classified as being localized to the interior or surface or as characteristic of any particular phonon mode. The chaotic nature of these vibrations is a direct result of the symmetry-lowering ligands and suggests that calculations that use pseudohydrogens in place of chemically reasonable ligands will provide a deceptively simple picture.

To quantitatively evaluate the observation that the ~200 cm^{-1} mode becomes more intense relative to the ~175 cm^{-1} mode at larger cluster sizes, we discard ligand motion and calculate the proportion of remaining total atomic displacement arising from interior cadmium and selenium atoms (Figure 5c). Values above 50% indicate vibrations that are more localized on interior cadmium and selenium atoms, and values less than 50% indicate vibrations that are more localized on surface cadmium atoms. Regardless of size, all clusters show more surface motion at lower energies and more interior motion at about 275 cm^{-1}. This result suggests that the higher energy peak at ~200 cm^{-1} in our Raman spectra reflects atomic motions that are more interior-like in nature while the lower energy peak at ~175 cm^{-1} reflects motions that are predominantly surface-like. Although we note that each mode involves motions of every atom regardless of type, consistent with calculations by Lin et al.,[29] we will from now on refer to the peak at ~175 cm^{-1} as a "surface" peak and the peak at ~200 cm^{-1} as an "interior" peak.

In light of these assignments, we can reexamine Figure 3. The trend of increasing interior and surface peak frequency with increasing particle size is consistent with the intuitive idea that atoms are more rigidly bound in larger clusters than they are in smaller clusters, especially for samples with such a large fraction of atoms at the surface. Interestingly, cluster ω_{int} values follow the same trend as LO values for the spherical nanocrystals, implying that the vibrations are similar in nature and evolve smoothly from molecular vibrations to the confined phonons of a strained lattice. Unlike the interior modes, the surface modes of the clusters, ω_{surf} = ~175 cm^{-1}, are substantially shifted to lower energy in comparison to the SO phonon mode at ~195 cm^{-1} seen in the Raman spectra of **CdSe**$_{(Wz\ NCs)}$. Although the SO mode has in some cases shifted to lower energy as nanocrystal size decreases, getting as low as 183 cm^{-1} for some samples,[53,54] others report the exact opposite trend,[23] making a clear determination of the relative contributions of phonon confinement and strain challenging. We believe that the surface peak observed for the clusters is qualitatively different from the SO feature, and its unusually low-energy results from a combination of factors, including the exceedingly small size of our samples and their nonspherical shape. There may even be a hint of the surface peak in the **CdSe**$_{(Wz\ NCs)}$ (d = 3 nm) spectra in Figure 2. Furthermore, the clusters have ligands on every surface atom, in contrast to larger, spherical nanocrystals that do not achieve full ligand coverage.[55] Rather than having frequencies similar to the SO mode, the clusters' surface mode frequencies instead approach values observed for the TO mode of **CdSe**$_{(Bulk)}$. However, TO modes are not typically observed in nanocrystal samples and are expected to decrease in energy with increasing particle size,[30] which is opposite to the trend we observe (Figure 3). Therefore, we conclude that ω_{surf} cannot be assigned to a TO mode.

The assignments also agree with the trend of increasing interior peak area relative to surface peak area with increasing cluster size shown in Figure 4. Because peak area is proportional to the sum of the Raman scattering cross section of each vibrational state contributing to that particular peak, both an increased number of contributing vibrational states and an increased Raman scattering cross section of each state can increase the Raman peak area. Our calculations indicate that the density of states of the interior modes does not increase with

DOI: 10.1021/jacs.6b10705
J. Am. Chem. Soc. 2016, 138, 16754−16763

cluster size faster than the surface state densities (Figure 5a), so we instead conclude that the Raman scattering cross section of the interior modes increases with respect to the surface modes with increasing cluster size. Because all cluster Raman measurements are nonresonant, precluding resonance effects from the explanation, we consider how the polarizability of surface and interior modes changes with cluster size. Past studies show that the average polarizability per atom increases with CdSe cluster size for clusters ranging from 12 to several hundred atoms, so as the surface area to volume ratio decreases with cluster size, the interior mode polarizability must increase relative to the surface mode polarizability.[56,57] Thus, the peak area ratio trend results from the increasing polarizability of interior modes in larger clusters.

The ligands also play an important role in determining the energies of the observed CdSe features. **CdSe**$_{(350\ nm)}$, **CdSe**$_{(380\ nm)}$, and **CdSe**$_{(408\ nm)}$ are passivated by a combination of *n*-butylamine and benzoate ligands, the latter of which are more rigid than the *n*-alkylcarboxylate or *n*-alkylphosphonate ligands typically found on nanocrystal surfaces.[35,58−60] Previous work on clusters capped by similarly rigid phenylthiolate ligands assigns low-energy Raman and infrared features in the region of 150−180 cm^{-1} to concerted stretching motions of the Cd−SPh bond where the phenylthiolate group is treated as a rigid unit.[4,32,33] Phenylthiolate (109.19 g/mol) and benzoate (121.12 g/mol) have a similar molecular weight, and visual inspection of DFT calculations[61] of the complex $Cd(O_2CPh)_2(NH_3)_2$ reveals low-energy vibrational modes in which benzoate moves as a rigid unit against cadmium, suggesting that similar motions on the surface of our clusters may contribute to the surface peak.

We have also tested the effect of ligands on cluster vibrational structure by performing DFT calculations on clusters with different arrangements of ligands. In symmetric ligation model 1, we place the ligands as evenly as possible on the smallest model cluster $Cd_{20}Se_{10}Cl_{20}(NH_3)_{20}$, with each vertex Cd atom of the tetrahedron possessing one Cl and two NH_3 ligands, each edge Cd atom possessing one Cl and one NH_3 ligand, and each facial Cd atom possessing a single Cl ligand (Figure S6a). In this way, we passivate each face with the same number of Cl and NH_3 ligands. Symmetric ligation model 2 is the same arrangement as model 1, but with one NH_3 ligand on each vertex swapped with a facial Cl. The asymmetric model possesses faces enriched in either Cl or NH_3 ligands (Figure S6b) and is much more polar and less stable than the symmetric models. The symmetric ligand distribution models possess very similar vibrational structures while the asymmetric arrangement affects the energy of motions of all atoms in the structure. This effect is obvious even for the motions of interior atoms not directly bound to ligands where the more asymmetric ligand arrangement results in a significant shift to lower energy (Figure 5d). Thus, an ensemble of clusters possessing a distribution of ligand binding motifs would exhibit vibrational features that are broadened and shifted to lower energy, and this effect should be magnified for particles with smaller dimensions. Following this reasoning, we attribute the breadth and low energy of the interior and surface peaks in part to heterogeneity of the ligand arrangements on individual clusters in a given sample. The same effects may also contribute to the line width of the lowest energy electronic transition, which broadens as the size decreases (Figure S1).

3.3. Variable-Temperature Measurements of CdSe Clusters. The phonon confinement and molecular approaches differ in their predictions of how vibrational peaks respond to changing temperature, so variable-temperature Raman experiments can, in principle, determine the size at which the vibrational structure of the clusters transitions from that of a molecule to a bulk material. A phonon confinement model predicts that the LO mode should narrow and shift to higher energy with decreasing temperature as a result of anharmonic effects.[1,5,25] This approach captures the temperature-dependent changes of nanocrystal vibrational spectra.[1,8,25,62,63] Anharmonic effects are dictated by the degree of phonon−phonon coupling and the magnitude of the thermal expansion coefficient.[63−65] Phonon−phonon coupling effects are more significant at higher temperatures and in many-atom species because there are more available resonant relaxation pathways with low coupling order under these conditions.[1,5,25] For bulk materials, higher temperatures generate a larger thermal population of excited phonons, increasing the number of scattering pathways for the optically excited phonon and resulting in a shorter vibrational lifetime and a broader peak. For molecules, the peak locations and widths should change little with temperature because there are far fewer relaxation pathways, and the peaks result from the summation of many discrete modes.[66] Even if lifetime effects cause the peak for each discrete mode to narrow, the overall peak, which is a sum of these modes, will remain close to its original width. In contrast to phonon−phonon coupling, thermal expansion is relevant for molecules as well as larger nanocrystals.

To evaluate which model better describes our samples, we performed variable-temperature Raman experiments. We use 532 nm excitation to measure Raman spectra for each cluster and $Cd(O_2CPh)_2(n\text{-}BuNH_2)_2$ between 78 and 296 K in approximately 50 K increments. Figure 6 displays spectra for **CdSe**$_{(350\ nm)}$ and **CdSe**$_{(408\ nm)}$. Cooling **CdSe**$_{(350\ nm)}$ produces a negligible change in the Raman spectrum, while, for **CdSe**$_{(408\ nm)}$, the interior mode shifts to higher energy and narrows, and the surface mode broadens, shifts to higher energy, and becomes less intense. The **CdSe**$_{(380\ nm)}$ spectral evolution is between **CdSe**$_{(350\ nm)}$ and **CdSe**$_{(408\ nm)}$ (Figure S7a), and the $Cd(O_2CPh)_2(n\text{-}BuNH_2)_2$ spectrum shows no change in the weak peak at ∼200 cm^{-1} with decreasing temperature, while the large background peak at ∼100 cm^{-1} decreases in intensity (Figure S7b).

Consistent with our analysis of room-temperature spectra, we fit the variable-temperature Raman spectra to two Gaussians with a linear background. Figures 6 and S7 show representative fits for the variable-temperature spectra, and Table S3 contains the fit parameters. As shown in plots of the room- and variable-temperature fit results (Figures 3, 7, S5, and S8), ω_{int} increases with increasing cluster size and also increases with decreasing temperature, although the trend is more pronounced for the larger clusters. $fwhm_{int}$, on the other hand, decreases with increasing size, and upon cooling remains constant for **CdSe**$_{(350\ nm)}$, decreases by 5 cm^{-1} for **CdSe**$_{(380\ nm)}$, and decreases by 9 cm^{-1} for **CdSe**$_{(408\ nm)}$. Although a clear temperature dependence of the cluster vibrational features exists, they respond differently depending upon size and neither a molecular nor a phonon confinement approach independently explains all the data. We examine the size dependence of these trends in more detail below.

Kusch et al. successfully applied a phonon confinement model with phonon−phonon coupling anharmonic effects to variable-temperature Raman spectra of 3.1, 4.8, and 7.8 nm diameter nanocrystals, along with bulk CdSe.[25] Chen et al. did the same over a smaller temperature range, but also incorporated thermal

DOI: 10.1021/jacs.6b10705
J. Am. Chem. Soc. 2016, 138, 16754−16763

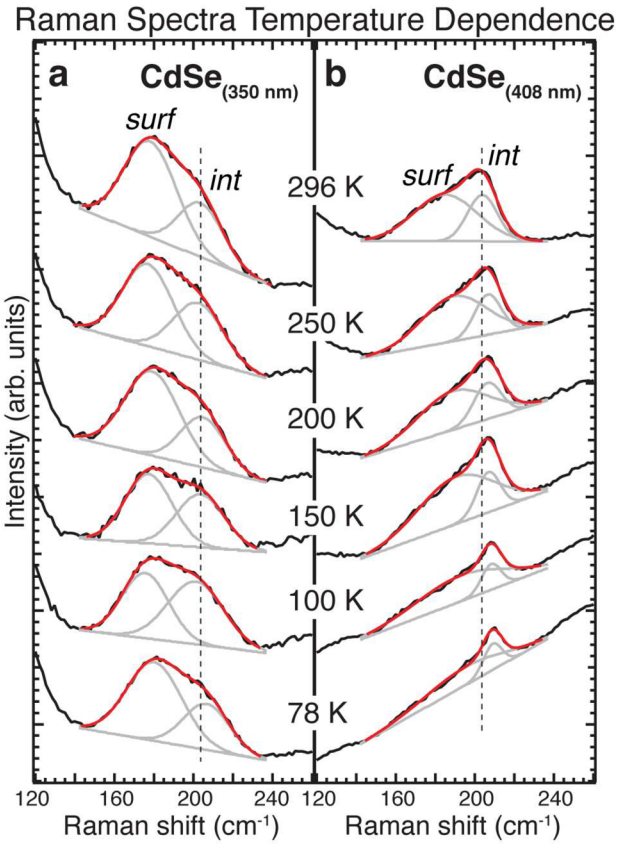

Figure 6. Representative variable-temperature Raman spectra measured at λ_{exc} = 532 nm for (a) **CdSe**$_{(350\ nm)}$ and (b) **CdSe**$_{(408\ nm)}$. The black, gray, and red curves are the data, individual Gaussian fits, and total fit, respectively. The dashed line is centered on the higher energy peak at room temperature, to emphasize that this peak shifts to higher energy as **CdSe**$_{(408\ nm)}$ cools, in contrast to **CdSe**$_{(350\ nm)}$.

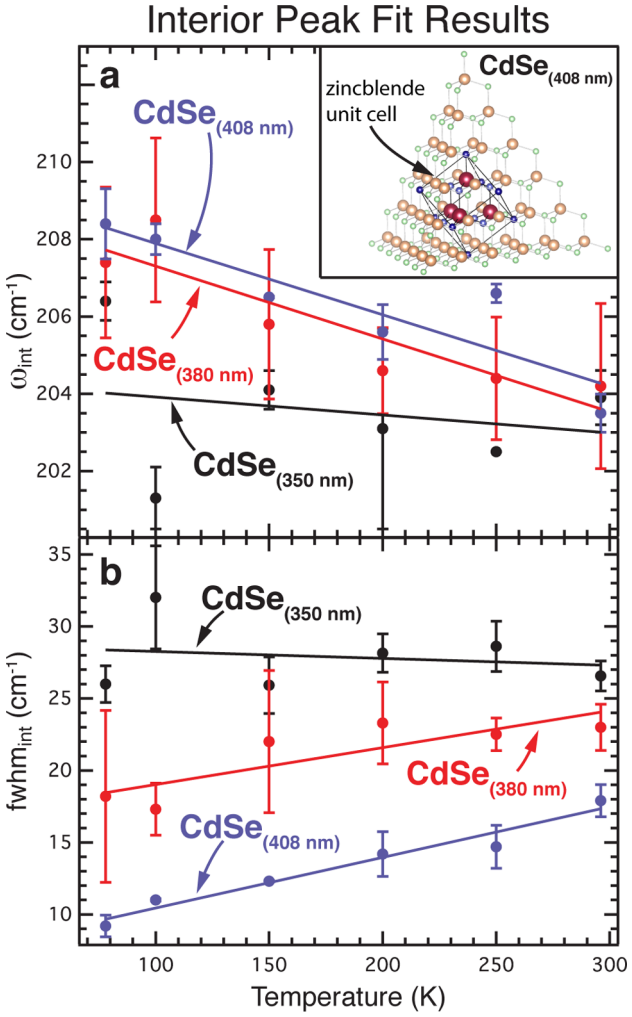

Figure 7. (a) The frequency and (b) fwhm of the interior peak from variable-temperature Raman spectra with λ_{exc} = 532 nm. **CdSe**$_{(350\ nm)}$, **CdSe**$_{(380\ nm)}$, and **CdSe**$_{(408\ nm)}$ are the black, red, and blue data, respectively. Solid lines are linear fits to the data. The fit equations are $\omega_{int,350} = -0.005T + 204$, $\omega_{int,380} = -0.019T + 209.2$, $\omega_{int,408} = -0.018T + 209.7$, $fwhm_{int,350} = -0.005T + 29$, $fwhm_{int,380} = 0.026T + 16$, and $fwhm_{int,408} = 0.035T + 6.9$. Error bars come from the standard deviation of fitting multiple spectra at the same temperature. The inset shows the single bulk zincblende unit cell contained within **CdSe**$_{(408\ nm)}$. Cadmium and selenium atoms in the unit cell are blue and purple, respectively.

expansion effects in their analysis.[62] In each case, the LO frequency increased and width decreased with decreasing temperature. For **CdSe**$_{(408\ nm)}$, with an edge length of 2.6 nm, ω_{int} increases from 204 to 208.5 cm^{-1} as temperature cools from 296 K to 78K while $fwhm_{int}$ decreases from 18 to 9 cm^{-1} over the same temperature range (Figure 7). These trends are in excellent agreement with those observed for the LO mode of the 3.1 nm diameter nanocrystal measured by Kusch et al. but offset to lower energy and broadened as expected for our smaller sample.[25] This agreement shows that the vibrations of **CdSe**$_{(408\ nm)}$ can be modeled with confined phonons, despite the fact that 53% of the cadmium and selenium atoms are on the cluster surface.

In contrast, for **CdSe**$_{(380\ nm)}$ the frequency and width of the interior and surface modes are less dependent on temperature and become nearly temperature independent for **CdSe**$_{(350\ nm)}$ (Figure 7 and S8). Our results are consistent with previous work by Dzhagan et al., who see a similar transition in cadmium sulfide nanocrystals; while the Raman features of 3.5 nm crystals are sensitive to temperature, 1.8 nm crystals do not exhibit a temperature response.[45] Since thermal expansion should still cause a shift in the vibrational frequency with temperature for molecules, we perform a simple calculation to test if the **CdSe**$_{(350\ nm)}$ data is reasonable. At higher temperatures, $(d\omega/dt) = -3\omega_0\gamma\alpha$ for thermal expansion.[64] Using ω_0 = 211 cm^{-1} from bulk CdSe,[20,21] the Gruneisen parameter γ = 1.1 for d = 4.5 nm zincblende CdSe nanocrystals,[67] and thermal expansion coefficient $\alpha = 8 \times 10^{-6}$ K^{-1} calculated for bulk zincblende CdSe,[68] we expect ω_{int} to decrease by 1.2 cm^{-1} from 77 to 296 K, showing that the small changes in ω_{int} for **CdSe**$_{(350\ nm)}$ can be explained by thermal expansion effects alone. The relative temperature insensitivity of the data for **CdSe**$_{(350\ nm)}$ shows that this cluster is best described by a molecular normal mode description. Thus, the vibrational structure of these clusters evolves from the molecular description for **CdSe**$_{(350\ nm)}$ to a confined phonon model for **CdSe**$_{(408\ nm)}$, with **CdSe**$_{(380\ nm)}$'s structure between these two limits. As a result, we identify the edge-length of **CdSe**$_{(380\ nm)}$, 2.1 nm, as the size at which the vibrational structure of CdSe clusters transitions from molecular vibrations to phonons.

To understand the transition from molecular to bulk vibrational properties, we consider the analogous evolution in CdSe electronic structure. The electronic structure's dependence on the nanocrystal radius r is governed by the exciton Bohr

DOI: 10.1021/jacs.6b10705
J. Am. Chem. Soc. 2016, 138, 16754−16763

radius α_{exc} = 56 Å.[69] When $r \gg \alpha_{exc}$, the electronic absorption spectrum is indistinguishable from bulk CdSe,[69] and bulk electronic bands exist. Nanocrystals with a radius on the order of or smaller than α_{exc} have a confined exciton and discretized conduction and valence band edges.[1] In the atomic limit, r approaches the lattice constant (6.052 Å for zincblende CdSe),[70] excitons are no longer meaningful, and a molecular electronic structure with fully discretized states exists.[3] Thus, transitions in the electronic structure from the bulk to nanocrystals and from nanocrystals to molecules occur at $d = 2\alpha_{exc}$ = 11.2 nm and $d = 2 \times 6.052$ Å = 1.2 nm, respectively.

We can similarly identify these transitions in the CdSe vibrational structure by focusing on the bulk LO mode. Many previous experiments have studied the size dependence of the vibrational structure, and the LO mode typically begins to shift to lower energy at d = 10 nm,[7,25] indicating that the phonons are now confined. Thus, the transition from bulk phonons to vibrational modes described by phonon confinement is at d = 10 nm and to molecular vibrations at d = 2.1 nm, as determined in this study. We interpret the first transition as the point at which the lattice structure is no longer large enough to accommodate the long wavelength, small k phonons probed by Raman spectroscopy. For d < 10 nm, true long-range, periodic phonons are no longer present, although the vibrations are well-described by a model which truncates the phonon vibrational wave functions at the nanocrystal boundaries. For d < 2.1 nm, this phonon-based description is no longer valid, since the cluster is now composed mostly of surface atoms, and a molecular description is necessary. The fraction of total cadmium and selenium atoms in the interior of our clusters is 0.38, 0.43, and 0.47 for **CdSe**$_{(350\ nm)}$, **CdSe**$_{(380\ nm)}$, and **CdSe**$_{(408\ nm)}$, respectively, showing that the boundary between a molecular and bulk vibrational structure occurs when roughly 43% of the nonligand atoms are in the interior of the cluster. Surprisingly, the vibrations of **CdSe**$_{(408\ nm)}$, with a 2.6 nm edge length, are well-described by a phonon-based model despite the fact that many truncated phonons would look similar in this size regime. We attribute the success of the phonon confinement model in **CdSe**$_{(408\ nm)}$ to its status as the smallest cluster that contains a full, bulk zincblende unit cell. Four tetrahedrally oriented corners of the cubic unit cell are on the cadmium atoms at the center of each cluster face (Figure 7a, inset, and Figure S9). Interestingly, the electronic and vibrational structure size transitions are not substantially different (electronic: d = 11.2 and 1.2 nm, vibrational: d = 10 and 2.1 nm), which is perhaps not surprising because the electronic potential energy surface determines the vibrational structure. In summary, for the bulk to nanocrystal transition, excitons and phonons become confined, and for the nanocrystal to molecular transition, excitons and phonons are no longer meaningful and molecular electronic and vibrational states exist.

4. CONCLUSION

We investigate the size dependence of the vibrational structure of a series of three atomically precise cadmium selenide clusters using Raman spectroscopy and density functional theory. Room-temperature Raman spectra have Cd−Se stretch peaks at 175 and 200 cm^{-1}. Density functional theory calculations of the motions of each cluster's normal modes show that these peaks are due to more surface-localized vibrations and interior-localized vibrations, respectively, in contrast to the more common surface optical and longitudinal optical phonon assignments. These calculations also show that the motions of ligand atoms, surface cadmium atoms, and interior cadmium and selenium atoms are all strongly coupled. The interior peak of the clusters evolves smoothly into the longitudinal optical phonon of the spherical nanocrystals, increasing in frequency with size. In contrast, the surface peak sharply increases in energy from tetrahedral **CdSe**$_{(408\ nm)}$ to spherical **CdSe**$_{(Wz\ NCs)}$, due to the different shape of the surface in each case. Variable-temperature Raman experiments show that the smallest cluster, **CdSe**$_{(350\ nm)}$, is well modeled by molecular vibrations while the largest cluster, **CdSe**$_{(408\ nm)}$, can be described by phonon confinement. This observation shows that the size boundary where the vibrational structure switches from a more molecular description to bulk phonons for cadmium selenide clusters is 2.1 nm, and the presence of a full bulk unit cell in **CdSe**$_{(408\ nm)}$ is necessary for successful application of a phonon confinement model.

■ ASSOCIATED CONTENT

Supporting Information

The Supporting Information is available free of charge on the ACS Publications website at DOI: 10.1021/jacs.6b10705.

Details on the preparation of octadecylphosphonic acid; sample absorbance and photoluminescence spectra; full Raman spectra of the clusters, the silicon substrate, and ligands; Cd$(O_2CPh)_2(n\text{-}BuNH_2)_2$ Raman spectra; room-temperature CdSe cluster fitting results for peak widths; models of $Cd_{20}Se_{10}Cl_{20}(NH_3)_{20}$ with different ligand arrangements (symmetric model 1 and asymmetric model in Figure 5d); variable-temperature Raman spectra for **CdSe**$_{(380\ nm)}$ and Cd$(O_2CPh)_2(n\text{-}BuNH_2)_2$; variable-temperature CdSe cluster fitting results for the surface peak; a larger image of **CdSe**$_{(408\ nm)}$ with the bulk unit cell superimposed; and details on our fitting approach with fit parameter tables (PDF)

■ AUTHOR INFORMATION

Corresponding Author

*acrowthe@barnard.edu

ORCID

Jonathan S. Owen: 0000-0001-5502-3267

Andrew C. Crowther: 0000-0003-2696-3211

Notes

The authors declare no competing financial interest.

■ ACKNOWLEDGMENTS

We thank Nilam Patel for assistance with Raman measurements, and Peter Chen and Nicholas Anderson for assisting with sample preparation. We also thank Yinsheng Guo, Omer Yaffe, and Louis Brus for lending us the cyrostat and providing instruction on its operation. A discussion with Irving Herman about the variable-temperature spectra was invaluable. A.N.B. and J.S.O. thank the National Science Foundation (NSF-CHE-1151172) for supporting work on cluster synthesis and characterization. A.C.C. thanks the Sally Chapman Fund and the Barnard College Office of the Provost for support.

■ REFERENCES

(1) Alivisatos, A. P. *J. Phys. Chem.* **1996**, *100*, 13226.

(2) Bawendi, M. G.; Steigerwald, M. L.; Brus, L. E. *Annu. Rev. Phys. Chem.* **1990**, *41*, 477.

(3) Gaponenko, S. V. In *Optical Properties of Semiconductor Nanocrystals*; Cambridge University Press: Cambridge, UK, 1998; p 27.

DOI: 10.1021/jacs.6b10705
J. Am. Chem. Soc. 2016, 138, 16754−16763

(4) Løver, T.; Bowmaker, G. A.; Seakins, J. M.; Cooney, R. P. *Chem. Mater.* **1997**, *9*, 967.
(5) Richter, H.; Wang, Z. P.; Ley, L. *Solid State Commun.* **1981**, *39*, 625.
(6) Rossetti, R.; Nakahara, S.; Brus, L. E. *J. Chem. Phys.* **1983**, *79*, 1086.
(7) Tanaka, A.; Onari, S.; Arai, T. *Phys. Rev. B: Condens. Matter Mater. Phys.* **1992**, *45*, 6587.
(8) Shiang, J. J.; Risbud, S. H.; Alivisatos, A. P. *J. Chem. Phys.* **1993**, *98*, 8432.
(9) Beecher, A. N.; Yang, X.; Palmer, J. H.; LaGrassa, A. L.; Juhas, P.; Billinge, S. J. L.; Owen, J. S. *J. Am. Chem. Soc.* **2014**, *136*, 10645.
(10) Baranov, A. V.; Rakovich, Y. P.; Donegan, J. F.; Perova, T. S.; Moore, R. A.; Talapin, D. V.; Rogach, A. L.; Masumoto, Y.; Nabiev, I. *Phys. Rev. B: Condens. Matter Mater. Phys.* **2003**, *68*, 165306.
(11) Tschirner, N.; Lange, H.; Schliwa, A.; Biermann, A.; Thomsen, C.; Lambert, K.; Gomes, R.; Hens, Z. *Chem. Mater.* **2012**, *24*, 311.
(12) Todescato, F.; Minotto, A.; Signorini, R.; Jasieniak, J. J.; Bozio, R. *ACS Nano* **2013**, *7*, 6649.
(13) Lin, C.; Gong, K.; Kelley, D. F.; Kelley, A. M. *ACS Nano* **2015**, *9*, 8131.
(14) Alivisatos, A. P.; Harris, T. D.; Carroll, P. J.; Steigerwald, M. L.; Brus, L. E. *J. Chem. Phys.* **1989**, *90*, 3463.
(15) Klein, M. C.; Hache, F.; Ricard, D.; Flytzanis, C. *Phys. Rev. B: Condens. Matter Mater. Phys.* **1990**, *42*, 11123.
(16) Kelley, A. M. *J. Phys. Chem. Lett.* **2010**, *1*, 1296.
(17) For bulk wurtzite CdSe, $\Gamma_{opt} = A_1 + E_1 + 2E_2 + 2B_1$ at the zero momentum Γ point.
(18) Tell, B.; Damen, T. C.; Porto, S. P. S. *Phys. Rev.* **1966**, *144*, 771.
(19) Schreder, B.; Kiefer, W. In *Handbook of Raman Spectroscopy*; Lewis, I. R., Edward, H. G. M., Eds.; Taylor and Francis: New York, 2001; p 491.
(20) Hermann, C.; Yu, P. Y. *Phys. Rev. B: Condens. Matter Mater. Phys.* **1980**, *21*, 3675.
(21) Plotnichenko, V. G. *Fiz. Tverd. Tela* **1977**, *19*, 1705.
(22) Zhang, J. Y.; Wang, X. Y.; Xiao, M.; Qu, L.; Peng, X. *Appl. Phys. Lett.* **2002**, *81*, 2076.
(23) Hwang, Y.-N.; Park, S.-H.; Kim, D. *Phys. Rev. B: Condens. Matter Mater. Phys.* **1999**, *59*, 7285.
(24) Pejova, B. *J. Phys. Chem. C* **2013**, *117*, 19689.
(25) Kusch, P.; Lange, H.; Artemyev, M.; Thomsen, C. *Solid State Commun.* **2011**, *151*, 67.
(26) Vasilevskiy, M. I.; Trallero-Giner, C. *Phys. Status Solidi B* **2010**, *247*, 1488.
(27) Ruppin, R.; Englman, R. In *Light Scattering Spectra of Solids*; Wright, G. B., Ed.; Springer: Berlin Heidelberg, 1969; p 157.
(28) Roy, A.; Sood, A. K. *Phys. Rev. B: Condens. Matter Mater. Phys.* **1996**, *53*, 12127.
(29) Lin, C.; Kelley, D. F.; Rico, M.; Kelley, A. M. *ACS Nano* **2014**, *8*, 3928.
(30) Chamberlain, M. P.; Trallero-Giner, C.; Cardona, M. *Phys. Rev. B: Condens. Matter Mater. Phys.* **1995**, *51*, 1680.
(31) Han, P.; Bester, G. *Phys. Rev. B: Condens. Matter Mater. Phys.* **2012**, *85*, 041306.
(32) Dance, I. G.; Choy, A.; Scudder, M. L. *J. Am. Chem. Soc.* **1984**, *106*, 6285.
(33) Ueyama, N.; Sugawara, T.; Sasaki, K.; Nakamura, A.; Yamashita, S.; Wakatsuki, Y.; Yamazaki, H.; Yasuoka, N. *Inorg. Chem.* **1988**, *27*, 741.
(34) Group theory analysis shows that our smallest cluster with simple hydrogen atom ligands has $\Gamma_{vib} = 19A_1 + 9A_2 + 28E + 37T_1 + 48T_2$, with the 219 total modes of A_1, E, and T_2 symmetry being Raman active. This large number of modes stands in contrast to bulk CdSe, which has A_1 and E_1 optical phonon branches that are only Raman active near $k = 0$.
(35) Owen, J. S.; Park, J.; Trudeau, P.-E.; Alivisatos, A. P. *J. Am. Chem. Soc.* **2008**, *130*, 12279.
(36) Anderson, N. C.; Owen, J. S. *Chem. Mater.* **2013**, *25*, 69.
(37) Momma, K.; Izumi, F. *J. Appl. Crystallogr.* **2011**, *44*, 1272.
(38) Carbone, L.; Nobile, C.; De Giorgi, M.; Sala, F. D.; Morello, G.; Pompa, P.; Hytch, M.; Snoeck, E.; Fiore, A.; Franchini, I. R.; Nadasan, M.; Silvestre, A. F.; Chiodo, L.; Kudera, S.; Cingolani, R.; Krahne, R.; Manna, L. *Nano Lett.* **2007**, *7*, 2942.
(39) Bochevarov, A. D.; Harder, E.; Hughes, T. F.; Greenwood, J. R.; Braden, D. A.; Philipp, D. M.; Rinaldo, D.; Halls, M. D.; Zhang, J.; Friesner, R. A. *Int. J. Quantum Chem.* **2013**, *113*, 2110.
(40) Becke, A. D. *J. Chem. Phys.* **1993**, *98*, 5648.
(41) Hay, P. J.; Wadt, W. R. *J. Chem. Phys.* **1985**, *82*, 299.
(42) Lee, C. T.; Yang, W. T.; Parr, R. G. *Phys. Rev. B: Condens. Matter Mater. Phys.* **1988**, *37*, 785.
(43) Stephens, P. J.; Devlin, F. J.; Chabalowski, C. F.; Frisch, M. J. *J. Phys. Chem.* **1994**, *98*, 11623.
(44) Albrecht, A. C. *J. Chem. Phys.* **1961**, *34*, 1476.
(45) Dzhagan, V. M.; Valakh, M. Y.; Himcinschi, C.; Milekhin, A. G.; Solonenko, D.; Yeryukov, N. A.; Raevskaya, O. E.; Stroyuk, O. L.; Zahn, D. R. T. *J. Phys. Chem. C* **2014**, *118*, 19492.
(46) Green, J. H. S.; Kynaston, W.; Lindsey, A. S. *Spectrochim. Acta* **1961**, *17*, 486.
(47) Korobkov, V. S.; Zharikov, N. K. *J. Appl. Spectrosc.* **1973**, *19*, 1306.
(48) Klausberger, G.; Furić, K.; Colombo, L. *J. Raman Spectrosc.* **1977**, *6*, 277.
(49) Lewandowski, W. *Arch. Environ. Contam. Toxicol.* **1988**, *17*, 131.
(50) Voznyy, O.; Mokkath, J. H.; Jain, A.; Sargent, E. H.; Schwingenschlögl, U. *J. Phys. Chem. C* **2016**, *120*, 10015.
(51) Abuelela, A. M.; Mohamed, T. A.; Prezhdo, O. V. *J. Phys. Chem. C* **2012**, *116*, 14674.
(52) Scott, A. P.; Radom, L. *J. Phys. Chem.* **1996**, *100*, 16502.
(53) Trallero-Giner, C.; Debernardi, A.; Cardona, M.; Menéndez-Proupín, E.; Ekimov, A. I. *Phys. Rev. B: Condens. Matter Mater. Phys.* **1998**, *57*, 4664.
(54) Comas, F.; Trallero-Giner, C.; Studart, N.; Marques, G. E. *Phys. Rev. B: Condens. Matter Mater. Phys.* **2002**, *65*, 073303.
(55) Anderson, N. C.; Hendricks, M. P.; Choi, J. J.; Owen, J. S. *J. Am. Chem. Soc.* **2013**, *135*, 18536.
(56) Jha, P. C.; Seal, P.; Sen, S.; Agren, H.; Chakrabarti, S. *Comput. Mater. Sci.* **2008**, *44*, 728.
(57) Rabani, E.; Hetenyi, B.; Berne, B. J.; Brus, L. E. *J. Chem. Phys.* **1999**, *110*, 5355.
(58) Anderson, N. C.; Hendricks, M. P.; Choi, J. J.; Owen, J. S. *J. Am. Chem. Soc.* **2013**, *135*, 18536.
(59) Fritzinger, B.; Capek, R. K.; Lambert, K.; Martins, J. C.; Hens, Z. *J. Am. Chem. Soc.* **2010**, *132*, 10195.
(60) Owen, J. *Science* **2015**, *347*, 615.
(61) The DFT calculations for the complex were performed using the same method and basis set as for the clusters.
(62) Chen, L.; Rickey, K.; Zhao, Q.; Robinson, C.; Ruan, X. *Appl. Phys. Lett.* **2013**, *103*, 083107.
(63) Balkanski, M.; Wallis, R. F.; Haro, E. *Phys. Rev. B: Condens. Matter Mater. Phys.* **1983**, *28*, 1928.
(64) Doerk, G. S.; Carraro, C.; Maboudian, R. *Phys. Rev. B: Condens. Matter Mater. Phys.* **2009**, *80*, 073306.
(65) Menendez, J.; Cardona, M. *Phys. Rev. B: Condens. Matter Mater. Phys.* **1984**, *29*, 2051.
(66) Harris, D. C.; Bertolucci, M. D. *Symmetry and Spectroscopy: An Introduction to Vibrational and Electronic Spectroscopy*; Oxford University Press: New York, 1978.
(67) Alivisatos, A. P.; Harris, T. D.; Brus, L. E.; Jayaraman, A. *J. Chem. Phys.* **1988**, *89*, 5979.
(68) Verma, A. S.; Singh, R. K.; Rathi, S. K. *Phys. B* **2009**, *404*, 4051.
(69) Ekimov, A. I.; Hache, F.; Schanneklein, M. C.; Ricard, D.; Flytzanis, C.; Kudryavtsev, I. A.; Yazeva, T. V.; Rodina, A. V.; Efros, A. L. *J. Opt. Soc. Am. B* **1993**, *10*, 100.
(70) Nelmes, R. J.; McMahon, M. I. In *Semiconductors and Semimetals*; Suski, T., Paul, W., Eds.; Academic Press: San Diego, 1998; Vol. *54*, p 220.

DOI: 10.1021/jacs.6b10705
J. Am. Chem. Soc. 2016, 138, 16754−16763